Supporting Information for

In Situ Probing Molecular Intercalation in Two-Dimensional Layered Semiconductors

Qiyuan He,[†,‖] Zhaoyang Lin,[†,‖] Mengning Ding,[‡§] Anxiang Yin,[†] Udayabagya Halim,[†] Chen Wang,[‡] Yuan Liu,[‡§] Hung-Chieh Cheng,[‡] Yu Huang,[‡§] and Xiangfeng Duan[*,†,§]

[†]Department of Chemistry and Biochemistry, [‡]Department of Materials Science and Engineering, and [§]California NanoSystems Institute, University of California, Los Angeles, California 90095, United States.

[‖]Qiyuan He and Zhaoyang Lin contributed equally to this work.

*To whom correspondence should be addressed. E-mail: xduan@chem.ucla.edu

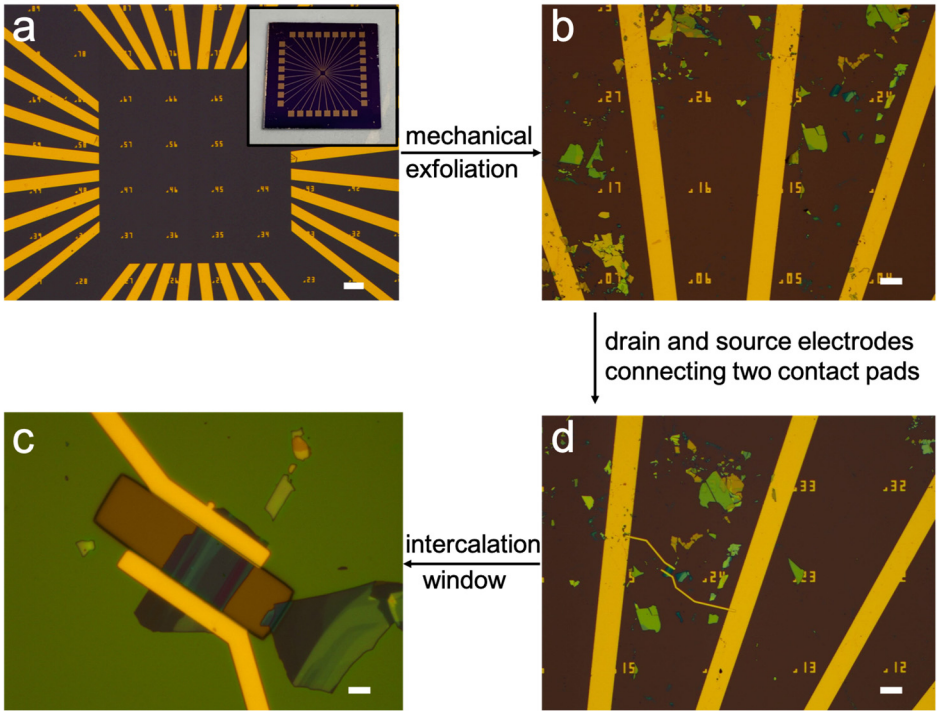

Figure S1. Fabrication of a two-terminal device for the microelectrochemical cell. (a) Pre-patterned Au contact pads. Inset: photo of the whole chip with 32 contact pads. Scale bar is 100 µm. (b) 2DLM nanosheets mechanically exfoliated on the chip. Scale bar is 50 µm. (c) Two terminal devices connecting a 2DLM nanosheet with two contact pads. Scale bar is 50 µm. (d) The reaction window for the electrochemical intercalation defined on a PMMA passivation defined by e-beam lithography. Scale bar is 5 µm.

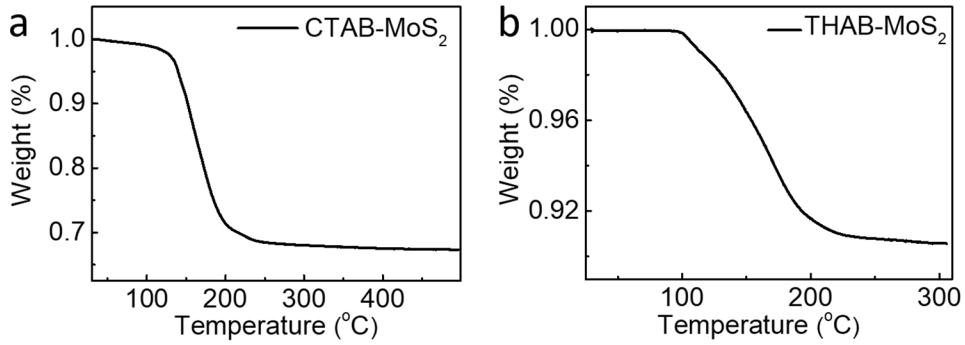

Figure S2. Thermogravimetric analysis (TGA) of (a) bulk CTAB-MoS_2 superlattice and (b) bulk THAB-MoS_2 superlattice. The molar ratio *x* represents not only the ratio of organic content inside the molecular superlattice but also the charge injection ratio into the MoS_2 lattice from the external circuit during the electrochemical intercalation. *x* is calculated to be 0.28 for CTAB intercalation and 0.02-0.04 for THAB intercalation, respectively.

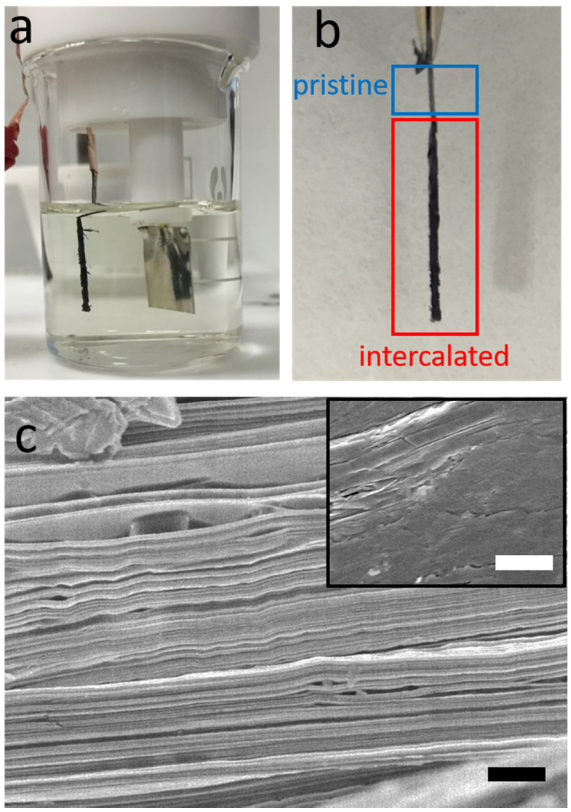

Figure S3. (a) Photograph of the electrochemical intercalation setup for the bulk crystal. (b) The intercalated thin piece crystal of MoS_2 showing the layer expansion. A typical two-electrode-electrochemical cell was used in our experiment, with bulk MoS_2 crystal as the cathode, Pt as the anode, and alkylammonium bromide in organic solvents (acetonitrile or N-Methyl-2-pyrrolidone) as the electrolyte. The resulting molecular superlattice was washed in acetonitrile and dried in vacuum before further characterizations. Alkylammonium cations were intercalated into *van der Waals* gaps of MoS_2 driven by the Coulomb force under reductive electrochemical potential, creating a stable molecular superlattice material. (b, c) Cross-sectional optical (b) and SEM (c) image of the intercalated MoS_2. Inset shows the cross-sectional SEM image of the pristine MoS_2. Scale bars are 10 μm.

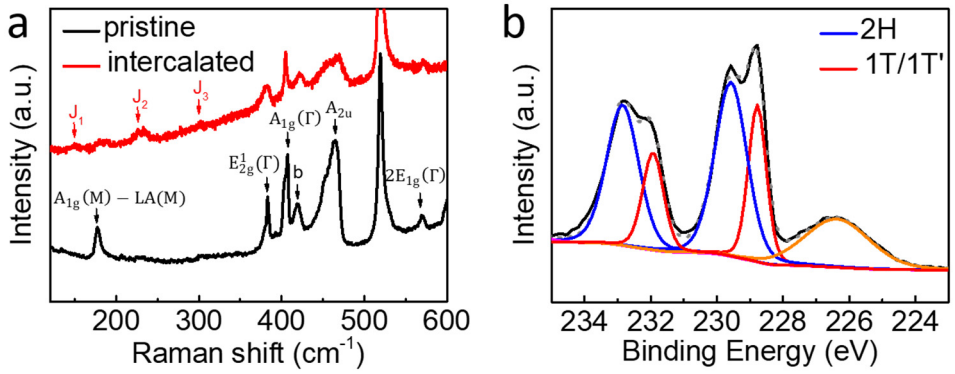

Figure S4. (a) Raman spectra of 5 nm MoS_2 nanosheet before and after the CTAB intercalation. The characteristic Raman peaks of semiconducting MoS_2 (A_{1g} (M)–LA(M), E^1_{2g}, and A_{1g}) become much weaker after the intercalation, which is commonly observed in intercalated MoS_2. New vibration peaks emerge at 150 cm^{-1} (J_1), 224 cm^{-1} (J_2), and 305 cm^{-1} (J_3) corresponds to characteristic peaks of metallic 1T/1T'-MoS_2. These peaks are relatively weak, consistent with lithium intercalated and exfoliated MoS_2 with mixed phases of 2H and 1T/1T'.[1] Also, the E^1_{2g} peak becomes broader, typically related to defects in the MoS_2 crystal structure as a result of the layer expansion. (b) XPS analysis on CTAB-MoS_2, showing the coexistence of semiconducting 2H (~ 71%) and metallic 1T/1T' (~ 29%) phases in the superlattice, with a significantly lower 1T/1T' portion than that of the lithium intercalation (typically > 70%).

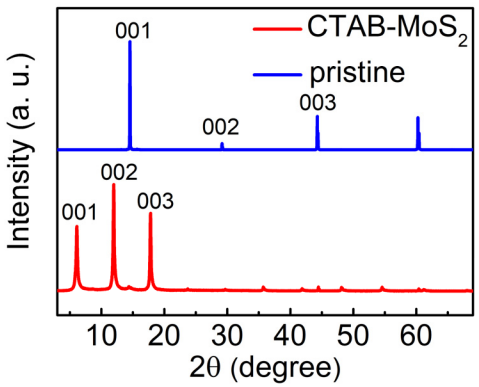

Figure S5. X-ray diffraction (XRD) patterns of pristine MoS_2 and CTAB-MoS_2 superlattice. The pristine MoS_2 shows the dominant (002) peak at $2\theta = 14.36$ degree, corresponding to an interlayer distance between *van der Waals* layers of 6.1 Å. While the fully intercalated CTAB-MoS_2 shows a much larger interlayer distance of 15.1 Å ($2\theta = 8.35$ degree).

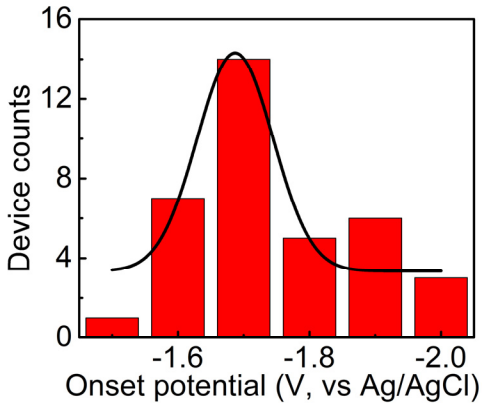

Figure S6. Statistics of the onset potentials of 36 independently recorded MoS_2 devices in ETS measurements during the CTAB intercalation. It suggests that the intercalation occurs within an electrochemical window (~ -1.7 ± 0.1 V *vs.* Ag/AgCl). The ETS signal is simultaneously affected by the thickness of the MoS_2 nanosheet, contact resistance between specific MoS_2 nanosheet and metal electrodes, exact geometric factor of the device, interfacial doping of the substrate, and many other parameters. Therefore, the onset potential values exhibit a relatively broad distribution.

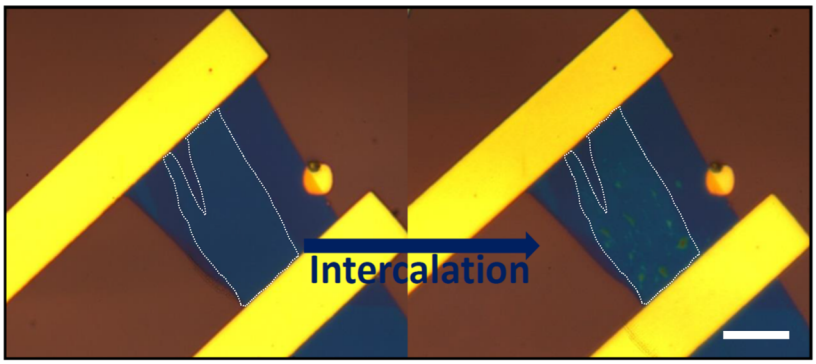

Figure S7. The optical image of thin layer MoS_2 after intercalation showing only the first layer (highlighted in white dash line) was intercalated by the CTA^+ cations. The clear color change is observed in the first layer after the carefully controlled intercalation. Scale bar is 5 μm.

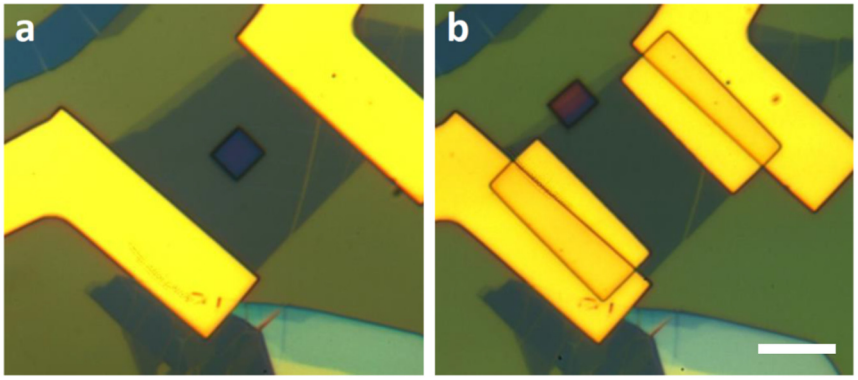

Figure S8. (a) MoS_2 with basal plane exposed to electrolyte during the molecular intercalation. (b) MoS_2 with edge exposed to electrolyte during the intercalation. By selectively exposing different area of the MoS_2 nanosheet to the electrolyte, we found that the intercalation occurs via the diffusion of organic cations at the edge of the nanosheet while the basal plane remains intact. In a MoS_2 device with only basal plane exposed to the alkylammonium solution during the electrochemical intercalation (a), no intercalation is observed in both *in situ* electrical signal and the optical observation. On the other hand, even a small exposure window at the edge of MoS_2 nanosheet (b) allows full electrochemical intercalation of the nanosheet, suggesting an efficient diffusion of the organic molecules through the decoupled MoS_2 layers. Scale bar is 5 μm.

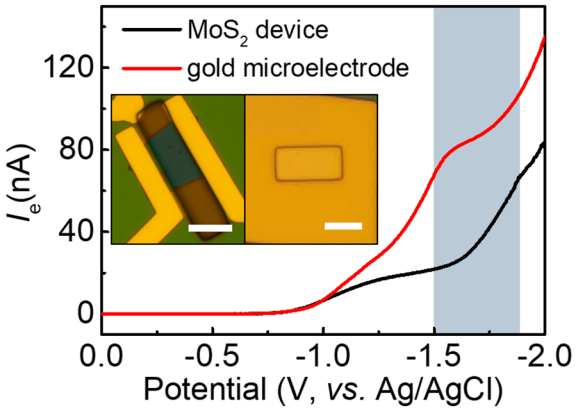

Figure S9. The electrochemical currents (I_e) of MoS_2 device during molecular intercalation vs a gold microelectrode in the same potential range in CTAB solution (5 mg/ml in NMP), showing comparable background electrochemical currents. The blue area indicates the molecular intercalation stage. Inset: optical images of the MoS_2 device (left) and the gold microelectrode (right). Scale bars are 10 μm. The scan rate of the electrochemical potential is 50 mV/s.

Specifically, a typical electron injection number in CTAB intercalation of MoS_2 nanosheet ((5-20 nm)×15 μm×5 μm)) is (2.2-8.8)×10^9 *e,* assuming a charge injection ratio of 0.28 (estimated from TGA measurements in Fig. S2a). At a scan rate of 50 mV/s, a typical intercalation process takes about 4-8 s (blue area in ETS profiles, 200 to 400 mV range), estimated from the conductance onset of the devices in ETS profiles. Therefore, the corresponding electrochemical current is about 0.08-0.64 nA, more than an order of magnitude lower than the background electrochemical current (tens of nA) within the same potential range (- 1.5 V to - 1.9 V *vs.* Ag/AgCl). Therefore, due to the relatively small number of charges injected during the intercalation process of microscopic devices and considerable background electrochemical current from side reactions (red curve. *i.e.*, the charge transfer process or electrochemical reactions on the surface of the working electrode, associated with the trace water and other chemical impurities in the electrolyte under high electrochemical potential), we are unable to directly extract the charge injection number from the electrochemical current profile.

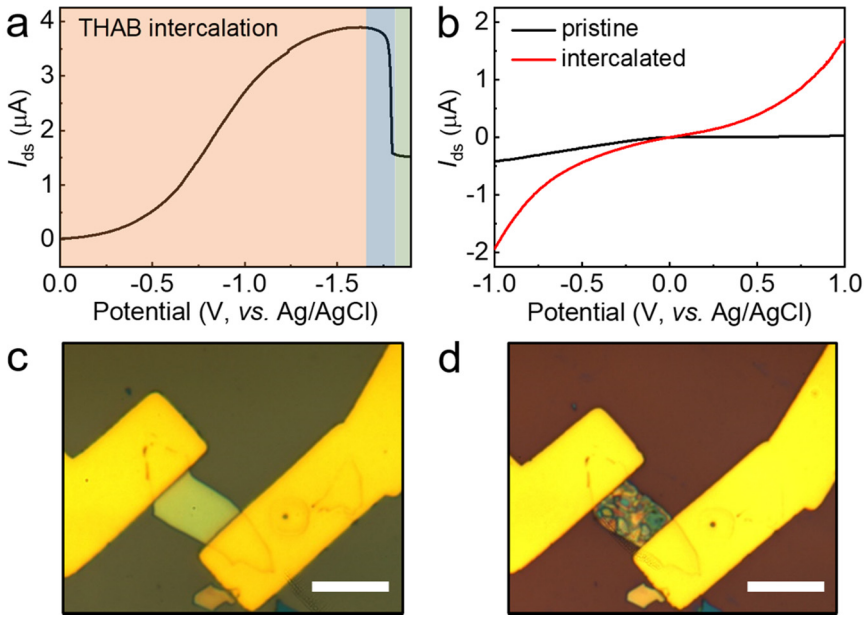

Figure S10. (a) ETS profile of the electrochemical intercalation of MoS_2 nanosheet with tetraheptylammonium bromide (THAB). The scan rate of the electrochemical potential is 50 mV/s. (b) Plots of I_{ds} *vs.* V_{ds} of a MoS_2 device before and after the THAB intercalation. (c,d) The MoS_2 device before (c) and after (d) the THAB intercalation. Scale bars are 10 μm. The THAB-MoS_2 superlattice is much more distorted than the CTAB-MoS_2 superlattice (see inset in Fig. 2a), possibly due to the bulky branched carbon chains of THAB molecules.

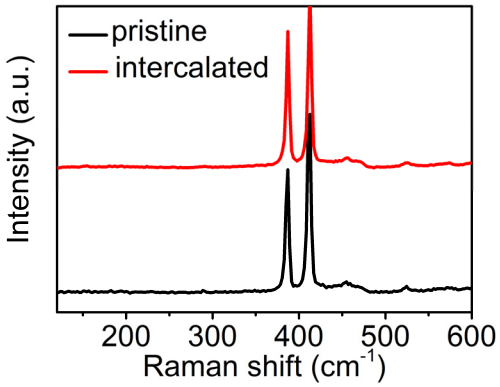

Figure S11. Raman spectra of MoS_2 nanosheet before and after the THAB intercalation.

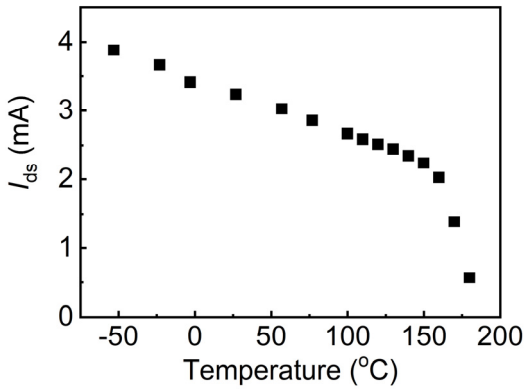

Figure S12. *In situ* monitoring of the I_{ds} *vs.* temperature of CTAB-MoS_2 device at V_{ds} = 0.5 V in vacuum, showing a drop of conductance above 150 °C. Each data point was collected after stabilizing at the target temperature for 30 min in a cryogenic probe station. The negative correlation below 150 °C agrees with the charge transport dominated by the metallic phase. The sharp drop upon exceeding 150 °C represents the evaporation of the organic intercalants and the phase-transition from metallic to semiconducting phase.

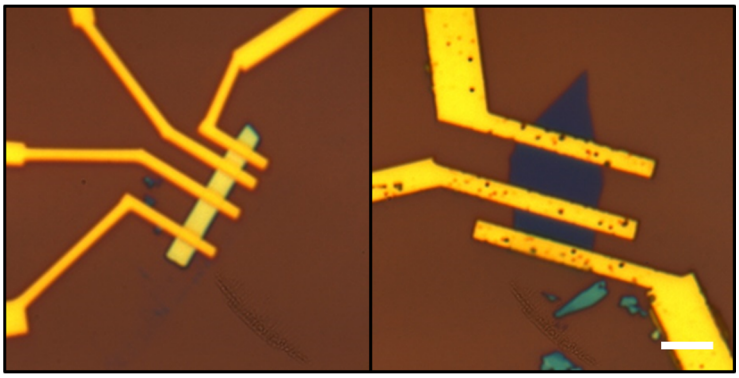

Figure S13. Typical devices based on transmission line measurement (TLM) to test the sheet resistance of the 2DLM nanosheets. Scale bar is 5 μm.

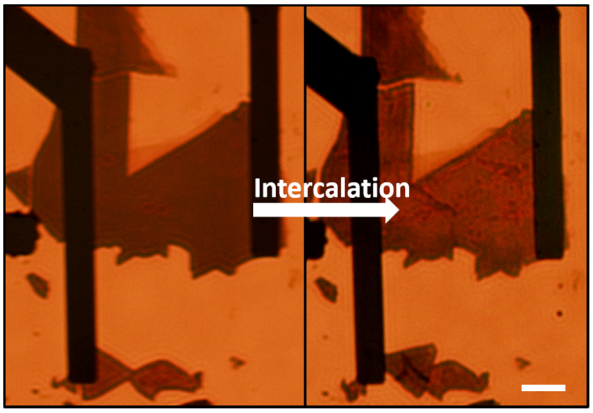

Figure S14. Optical image of typical MoS_2 nanosheet before and after the CTAB intercalation. The enhancement in transparency for the thick sample (> 10 nm) is visible on optical images. Scale bar is 5 μm.

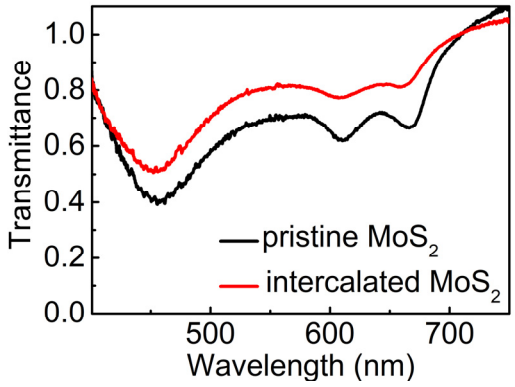

Figure S15. Transmittance spectra of 8 nm MoS_2 flake after CTAB intercalation.

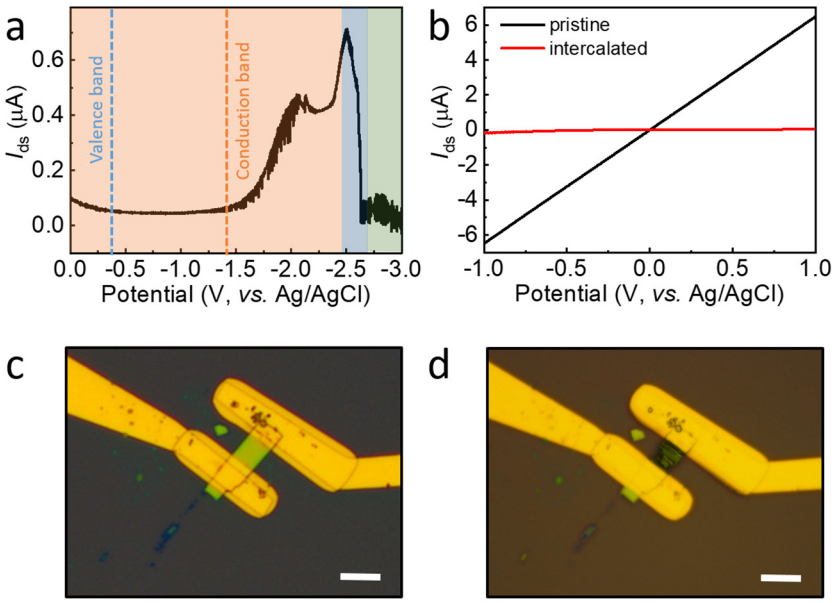

Figure S16. Electrochemical intercalation of $PdSe_2$. (a) ETS profile of the molecular intercalation of $PdSe_2$ nanosheet with CTAB. The scan rate of the electrochemical potential is 50 mV/s. The molecular intercalation of semiconductor occurs at the saturation region under ionic-gate modulation (pink area) where the Fermi level of the TMD nanosheet has been brought into the conduction band.[3] However, an additional potential barrier (> 1V) exists between the conduction band edge position and the intercalation onset potential. Therefore, the intercalation onset potential value is concurrently affected by (1) the conduction band edge position, (2) the energy difference between Fermi level and conduction band edge (*i.e.* doping level), and (3) possible additional kinetic overpotentials (4) the voltage drop on the material itself (depending on the conductivity of specific material) and contact region (depending on the contact resistance). (b) Plots of I_{ds} *vs* V_{ds} of the $PdSe_2$ device before and after the intercalation. (c,d) The optical images of the $PdSe_2$ nanosheet before (c) and after (d) the intercalation, showing strongly distorted structure after molecular intercalation. Scale bars are 5 μm. $PdSe_2$ has a widely tunable bandgap from metallic to ~ 1.3 eV.[2] The bandgap of $PdSe_2$ used in this experiment is estimated to be ~ 1 eV, determined by gap between the onset potential of *p*-and *n*-type regions in ionic gating, similar to the method to determine the bang gap of WS_2 nanosheet in ionic-gated field-effect transistor in previous report.[3]

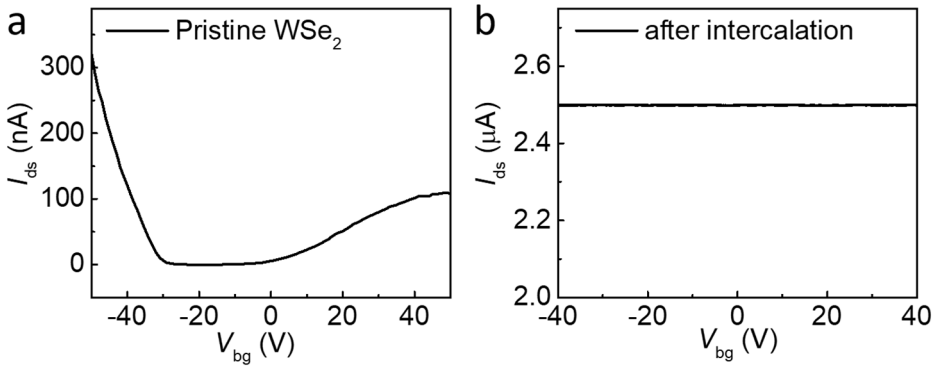

Figure S17. The back-gated measurements of a WSe_2 device before (a) and after (b) the molecular intercalation of CTAB. V_{ds} = 100 mV.

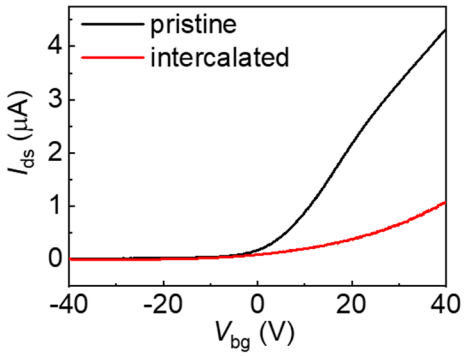

Figure S18. Plots of I_{ds} *vs.* V_{bg} of a 1T'-ReS_2 device before and after the intercalation, showing an *n*-type characteristic. V_{ds} = 100 mV.

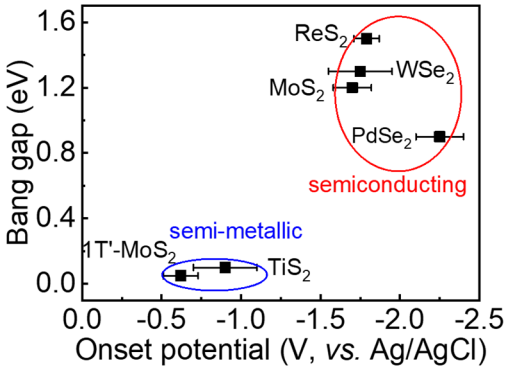

Figure S19. The onset potentials of CTAB intercalation of six different TMD materials at a scan rate of 50 mV/s. The standard deviation is obtained from 5 devices for each TMD. It is indicated that the molecular intercalation of metallic TMDs is generally much easier than that of semiconducting TMDs.

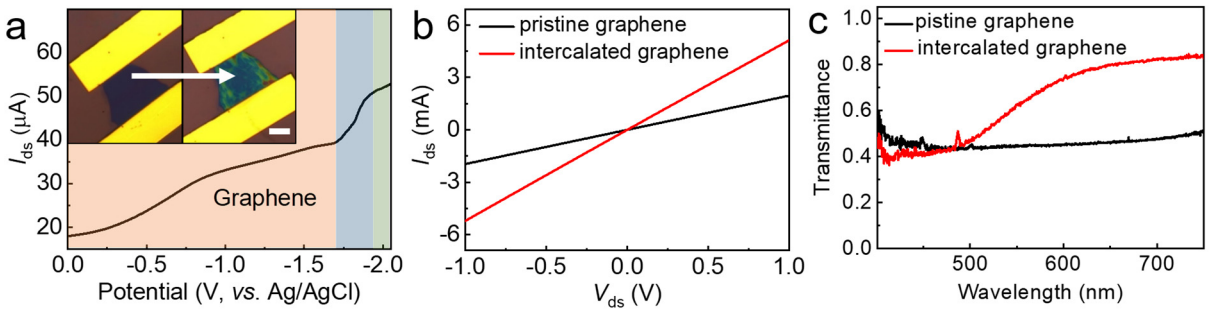

Figure S20. (a) ETS profile of the molecular intercalation of few-layer graphene nanosheet with CTAB. The inset shows the optical images of the few-layer graphene nanosheet before and after the intercalation. Scale bar is 5 μm. (b) Plots of I_{ds} *vs.* V_{ds} of a graphene device before and after the intercalation. (c) Transmittance spectra of 20-nm graphene before and after the CATB intercalation. The molecular intercalation of graphene shows a significant increase of transmittance in the visible range, similar to the intercalation of MoS_2. However, the detailed mechanism behind such dramatic change in optical properties remains elusive. With the excellent thermal and chemical stability of the intercalated superlattice, it may be a promising transparent electrode in the visible range.

References

1. Eda, G.; Yamaguchi, H.; Voiry, D.; Fujita, T.; Chen, M.; Chhowalla, M. Photoluminescence from Chemically Exfoliated MoS_2. *Nano Lett.* **2011,** *11*, 5111-5116.

2. Qin, D.; Yan, P.; Ding, G.; Ge, X.; Song, H.; Gao, G. Monolayer $PdSe_2$: A Promising Two-dimensional Thermoelectric Materials. *Sci. Rep.* **2017**. *8*, 2764.

3. Braga, D., Gutiérrez Lezama, I., Berger, H.; Morpurgo, A. F. Quantitative Determination of the Band Gap of WS_2 with Ambipolar Ionic Liquid-Gated Transistors. *Nano Lett.* **2012**. *12*, 5218-5223.